water

MDPI

Article

Evaluating the Effectiveness of Rainwater Storage Tanks Based on Different Enabling Rules

Yongwei Gong [1,*], Ge Meng [1], Kun Tian [1,2] and Zhuolun Li [1]

[1] Key Laboratory of Urban Stormwater System and Water Environment, Ministry of Education, Beijing University of Civil Engineering and Architecture, Beijing 100044, China; mengge0803@163.com (G.M.); tiank@ouchn.edu.cn (K.T.); lizhuolungk@163.com (Z.L.)

[2] The Party Committee in Colleges and Universities, The Open University of China, Beijing 100039, China

* Correspondence: gongyongwei@bucea.edu.cn

Abstract: A proposed method for analyzing the effectiveness of rainwater storage tanks (RWSTs) based on various enabling rule scenarios has been proposed to address the issue of incomplete strategies and measures for controlling excessive rainwater runoff. Three enabling rules for RWSTs have been proposed, as follows: enabling rule I, which involves activation upon rainfall; enabling rule II, which requires the rainfall intensity to reach a predetermined threshold; and enabling rule III, which necessitates the cumulative rainfall to reach a set threshold. In order to assess the effectiveness of these enabling rules when reducing the total volume of rainwater outflow (TVRO), peak flow rate (PFR), and peak flow velocity (PFV), a comparative analysis was conducted to determine which enabling rule yielded the most optimal control effect. The findings indicate that the enabling rule I is responsible for determining the optimal unit catchment's rainfall capture volume (UCRCV), which is measured at 300 $m^3 \cdot ha^{-1}$. Additionally, the control effect of the TVRO of the RWSTs remains largely unaffected by the peak proportion coefficient. Enabling rule II establishes the optimal activation threshold at a rainfall intensity of 1 $mm \cdot min^{-1}$; under this enabling rule, RWSTs demonstrate the most effective control over PFR and PFV. Enabling rule III enables the determination of the optimal activation threshold, which is set at a cumulative rainfall of 20 mm; under this enabling rule, the implementation of the RWST technique yields the most effective control over the TVRO. Consequently, the optimal rainwater runoff reduction plan for the study area has been successfully determined, providing valuable guidance for the implementation of scientific and reasonable optimal runoff management.

Keywords: rainwater storage tanks (RWSTs); peak flow control; rainwater runoff; rainwater and flood control

Citation: Gong, Y.; Meng, G.; Tian, K.; Li, Z. Evaluating the Effectiveness of Rainwater Storage Tanks Based on Different Enabling Rules. *Water* **2024**, *16*, 787. https://doi.org/10.3390/w16050787

Academic Editor: Marco Franchini

Received: 3 February 2024
Revised: 28 February 2024
Accepted: 5 March 2024
Published: 6 March 2024

1. Introduction

With the acceleration of urbanization in recent years, impermeable pavement is gradually replacing natural permeable pavement, leading to a significant decrease in urban soil permeability [1,2]. Additionally, in recent years, extreme rainfall events have begun to occur more frequently, posing significant risks to the flood control and drainage capacities of cities [3,4]. Flood disasters have some of the most devastating impacts among natural disasters in terms of economic losses and population deaths [5]. Between 2000 and 2019, flood disasters accounted for 31% of the global economic losses caused by natural disasters, with an economic loss of USD 651 billion [6,7]. Floods have an impact on both developed and developing countries [8]. Among these, China has some of the most severe flooding disasters in the world, with about two-thirds of its territory facing the threat of flooding and many of its cities suffering as a result [9]. According to the China Flood and Drought Disaster Prevention Bulletin 2022, a total of 33.8526 million people were affected by floods in 2022, resulting in direct economic losses of RMB 128.899 billion [10]. Urban flooding has become a prominent issue affecting urban public safety in China and a major obstacle to sustainable urban development, and in turn has attracted high attention from the country [11–13]. The investigation of urban water safety has emerged as a prominent subject of scholarly inquiry on a global scale. Developed nations and regions have devised a range of robust theoretical and technical frameworks for urban rainwater and flood management, aiming to address the issue of urban waterlogging and to attain urban water security [14]. China has progressively implemented a sponge city urban rainwater management system, centered around low impact development, and has successfully devised engineering technologies and equipment for "source reduction, process control, and system governance". This has significantly contributed to the mitigation of the issue of urban waterlogging [11,15].

At present, research has shown that low impact development (LID) facilities are still effective in controlling the rainwater runoff generated by small- and medium-sized rainfall events, but are basically ineffective when alleviating the urban waterlogging caused by large amounts of rainfall [16,17]. In the work of waterlogging control, RWSTs are often used to collect and retain rainwater runoff to alleviate waterlogging problems. Many scholars have conducted research on the structural design, operational efficiency optimization, and control strategies of RWSTs. For example, Zhang et al. [18] have developed an underground RWST using fiber-reinforced polymer materials for rainwater retention, storage, and reuse to alleviate urban waterlogging and collect rainwater. Dabrowski et al. [19] have examined the impact of the outflow structure of RWSTs on the necessary volume of the system. The authors introduced a reasonable method for determining the size of RWSTs suitable for small-scale sewage treatment systems. Their aim was to demonstrate that the volume of an RWST remains unaffected by the configuration of the effluent discharge from the tank. Wang et al. [20,21] have devised a novel approach that employs the stormwater management model (SWMM) and an elastic feature measurement-based method to minimize the modeling prerequisites in order to seek optimization solutions for RWSTs. The primary objective is to minimize the occurrence of flooding, reduce the total suspended solids load, and minimize storage costs to the maximum extent feasible. The proposed multi-objective optimization framework has the potential to identify the most optimal solution for an RWST or LID. This methodology offers a novel approach for determining improved RWST layout schemes and contributes valuable insights for equipment placement in sustainable drainage systems. Wang et al. [22] have proposed a method to optimize the simulation accuracy of RWST operating scenarios in the SWMM, determined the real-time control (RTC) rules and RWST operating modes for different scenarios of RWSTs in the SWMM (flushing toilets, green space irrigation, combined flushing toilets and green space irrigation). They also evaluated the multi-objective operating effect of residential scale RWSTs. This study improved the simulation accuracy of the model and established a multi-objective evaluation method for operational effectiveness, providing theoretical support for the optimization method for the operational strategy of RWSTs. However, there is still a lack of optimal control strategies for rainwater runoff at the large watershed scale, and especially of methods for determining RTC schemes for RWSTs, which still require sufficient research.

In summary, there is currently a knowledge gap in research on methods and technical systems for controlling excessive rainwater runoff. Exploring the optimal timing and conditions for RWSTs to collect rainwater runoff is of great significance. Therefore, this study proposes a method by which to optimize the threshold for RWST activation—a method that utilizes the InfoWorks integrated catchment management (ICM) model—and takes a specific urban watershed in Jinan city as an example for research. The control effect of RWSTs on rainwater runoff under different rainfall conditions and different enabling rules was studied. The optimal enabling rules and corresponding activation thresholds were evaluated and obtained in order to obtain the optimal RTC scheme for runoff control in the study area so as to provide a theoretical basis and a runoff control technology system for future waterlogging control and urban disaster prevention work in the study area.

2. Methodology

2.1. Study Area

The research site is situated in Jinan city, Shandong province, specifically within the Shiqingya river basin, which is a sub-basin of the Xingji river basin. Encompassing an approximate area of 5.45 km^2, the Shiqingya river basin constitutes 14% of the designated pilot area. The total area of the building is 0.49 km^2, the road square area is 1.66 km^2, the park green area is 0.65 km^2, and the mountain area is 2.66 km^2. The Shiqingya river, situated within the aforementioned watershed, functions as the principal tributary to the Xingji river. The confluence of the Shiqingya and Xingji rivers has been designated as the control point for the watershed, wherein the investigation of rainwater runoff control is conducted. The geographical position of the study area is depicted in Figure 1.

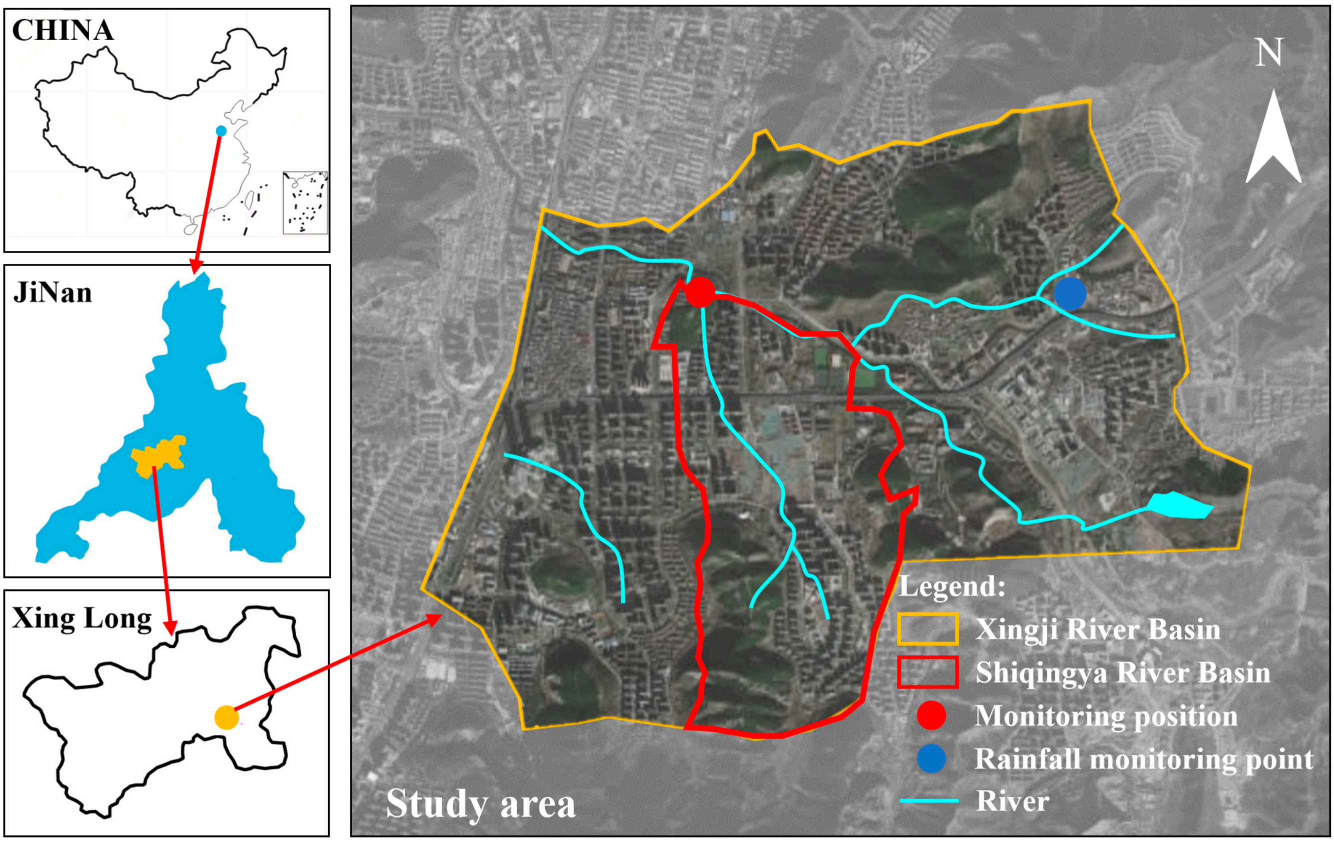

Figure 1. Location of the study area.

2.2. Model Building

2.2.1. Multi Model Coupling

The study area was simulated and analyzed using the InfoWorks ICM model. However, the independent models of InfoWorks ICM do not provide a comprehensive representation of the entire rainfall runoff flow scenario in terms of two-dimensional surface, drainage network, and river channels. Consequently, it becomes imperative to integrate the surface runoff model, pipeline convergence model, two-dimensional surface overflow model, and river confluence model (Figure 2) in order to accurately simulate the water exchange process between various sub models. The watershed can be partitioned by considering various factors, such as the topography, local slope orientation, and spatial arrangement of the river system, alongside urban planning and land utilization patterns, road network development, and the intended drainage network.

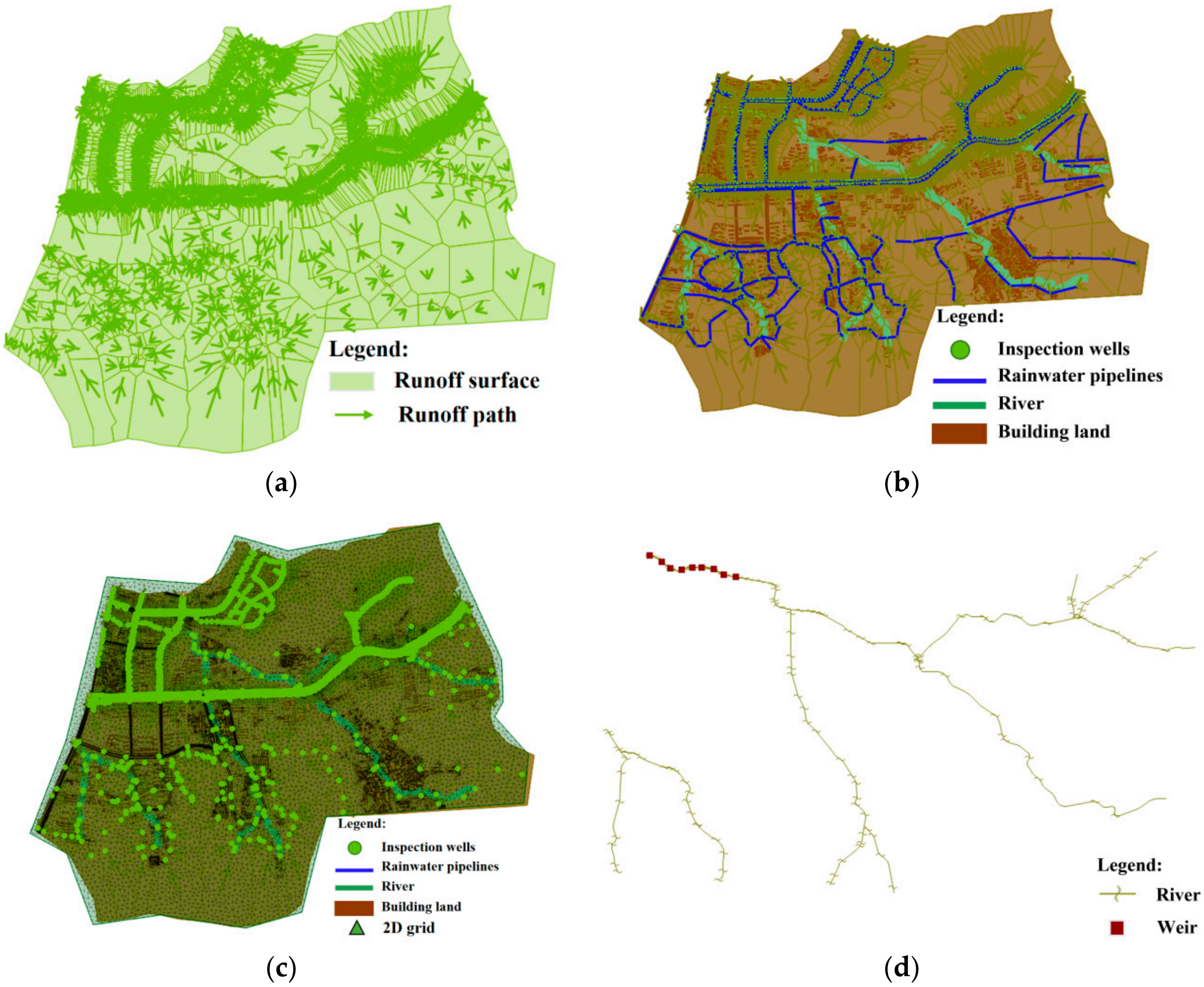

Figure 2. Multi model coupling: (**a**) surface runoff model, (**b**) network convergence model, (**c**) ground surface flowing model of 2D, and (**d**) river confluence model.

The current water system, ditches, and pipeline network data in the study area were vectorized and subsequently imported into the InfoWorks ICM model to generate the topological structure diagram of the pipeline network in the research basin. In order to enhance the precision of the InfoWorks ICM model's simulation, the Tyson polygon method, integrated within the model, was employed to subdivide the 9 catchment areas into 1271 sub-catchment areas, aligning with the configuration of the rainwater pipeline network. The research basin encompasses a total of 7 generalized drainage outlets, 1351 inspection wells, and 1202 rainwater pipelines. The existing pipeline network comprises circular pipes with diameters ranging from 300 mm to 1500 mm, square culverts with widths ranging from 700 mm to 7500 mm, and spans a total length of 66.32 km.

2.2.2. Design Scheme for the Enabling Rule of RWSTs

Constructing RWSTs to retain rainwater in areas with severe waterlogging can effectively reduce the total volume of rainwater outflow (TVRO) and peak flow rate (PFR) [23]. Thus, when studying regional waterlogging control, the potential location for constructing RWSTs should be determined based on the waterlogging conditions in the study area. Therefore, based on the simulation results of waterlogging points in the study area, the potential locations for the construction of five new RWSTs are shown in Figure 3.

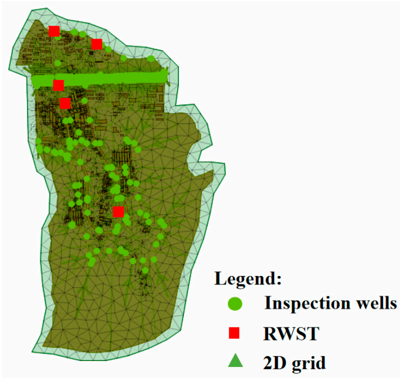

Figure 3. Location of RWSTs.

By using RTC technology on RWSTs, the PFR reduction rate can be further improved [23,24]. This study primarily investigates the operational guidelines of RWSTs under various enabling rules and assesses their impact on rainwater runoff control. The discharge mechanism of RWSTs is simplified, wherein organized emissions are executed subsequent to the conclusion of rainfall. There exist three distinct regulations governing the activation of RWSTs:

(1) Enabling rule I: Initiate activation promptly upon the start of rainfall.

At the onset of precipitation, the RWST is set into motion, allowing rainwater runoff to infiltrate the system via terrain slopes, nodes, pipelines, and other conduits. When the RWST reaches its maximum capacity or when rainfall ceases, it ceases to store water. Enabling rule I establishes six threshold values for the unit catchment's rainfall capture volume (UCRCV), namely 0, 100, 200, 300, 400, and 500 $m^3 \cdot ha^{-1}$, which corresponds respectively to RWST volumes of 0, 5.45×10^4, 10.90×10^4, 16.35×10^4, 21.80×10^4, and 27.25×10^4 m^3. These values are used to investigate the functioning of the regulating RWST under various UCRCV conditions and to determine the most suitable UCRCV for the optimal performance of RWST.

(2) Enabling rule II: Rainfall intensity reaches threshold.

The process of rainfall is characterized by its dynamic nature, whereby the activation of the RWST occurs when the rainfall intensity surpasses a predetermined threshold. Rainwater runoff is directed into the RWST through various pathways. The storage of water in the RWST ceases either when it reaches its maximum capacity or when the rainfall ceases altogether. Enabling rule II establishes six distinct thresholds for rainfall intensity, namely 0, 1.0, 2.0, 3.0, 4.0, and 5.0 $mm \cdot min^{-1}$. The primary objective of this enabling rule is to investigate the functioning of the RWST under different activation conditions based on rainfall intensity, ultimately determining the most optimal threshold for activating the RWST.

(3) Enabling rule III: Cumulative rainfall reaches threshold.

Once the cumulative rainfall surpasses the predetermined threshold, the RWST is triggered, allowing rainwater runoff to enter. The storage process ceases either when the RWST reaches its maximum capacity or when the rainfall ceases. Enabling rule III establishes six distinct cumulative rainfall thresholds (0, 20, 40, 60, 80, and 100 mm) by which to investigate the RWST's functionality under various activation conditions and to identify the most effective cumulative rainfall threshold for RWST activation.

The three enabling rules above are commonly used RTC modes for RWSTs in practical engineering. Each enabling rule is set with six different thresholds. Through flood simulation using the InfoWorks ICM model, the optimal enabling rule and threshold for solving waterlogging points in the study area will be determined, providing the optimal runoff reduction scheme for future waterlogging control work.

2.3. Rainfall Parameters

The short-duration rainfall process line in this study employs the commonly utilized Chicago rain pattern, with a duration of 120 min. As per *the Comprehensive Planning of Urban Drainage (Rainwater) and Waterlogging Prevention in Jinan*, [25] the modified rainstorm intensity Equation (1) for Jinan is presented below:

$$q = \frac{1421.481 \times (1 + 0.932 lgP)}{(t + 7.347)^{0.617}} \tag{1}$$

where, q is the design rainstorm intensity, mm·min^{-1}; P represents the design return period, a; t is the time it takes for the rainwater well to collect rainwater (which is related to the surface collection time and the time it takes for rainwater to pass through the pipeline, and is designed by the model based on parameters such as terrain, slope, and pipeline length) in minutes.

Calculate and select two types of rainfall data using Equation (1) to simulate the operational effectiveness of RWSTs under different enabling rule scenarios: (1) rainfall with a return period of 1, 3, 5, 10, 20, and 50 years (every 5 min interval represents the time interval between changes in rainfall intensity, the smaller the time interval, the closer it is to the actual rainfall scenario) and a peak rainfall coefficient (the ratio of the time elapsed from the onset of rainfall to its peak intensity to the total duration of the rainfall event) of 0.3 (P =1, 3, 5, 10, 20, 50, r = 0.3); (2) rainfall with a return period of 20 years (every 5 min interval) and peak rainfall coefficients of 0.3, 0.5, and 0.7 (P = 20a, r = 0.3, 0.5, 0.7). Table 1 and Figure 4 show short-term rainfall patterns with different rainfall return periods and peak coefficients. From Figure 4, it can be seen that, as the return period increases, rainfall depth and intensity increase. With the increase of the rainfall peak coefficient, the corresponding time of rainfall peak intensity shifts backward, and the accumulated rainfall before the rainfall peak (the area formed by the rainfall intensity curve and the x-axis) increases. Therefore, by selecting the above two types of rainfall data to simulate the rainwater runoff control effect in the study area, the relationship between rainfall, rainfall intensity, and cumulative rainfall before rainfall peak and the rainwater runoff control effect can be compared. Furthermore, by orthogonal combination and comparison with three enabling rules, the optimal enabling rules and thresholds can be determined based on the effectiveness of rainwater runoff control. In addition, in the preliminary work, the flow rate and velocity hydrographs of monitoring locations under three enabling rules (a total of 162 simulation scenarios) in the model were exported. It was found that the relationships between flow rate, velocity changes, peak delay time and return period at the monitoring location were relatively ideal, and, after comparison, there were no sudden increases or decreases. Due to the large number of flow rate and velocity hydrographs, TVRO, PFR, and peak flow velocity (PFV) were selected for comparison in each scenario in order to improve the comparison efficiency between simulated scenarios and to obtain more scientific conclusions.

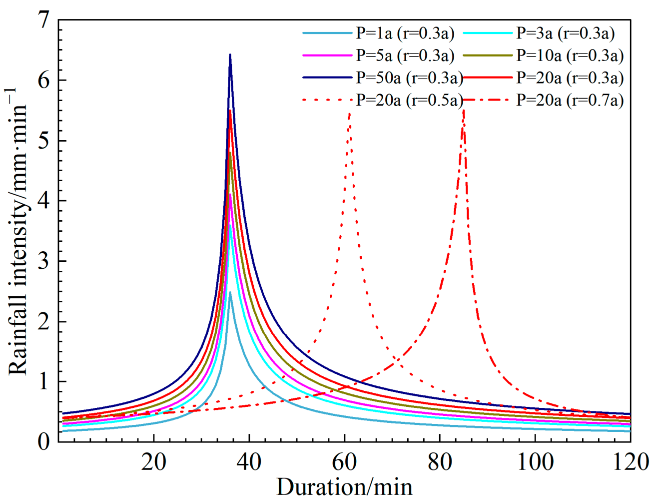

Figure 4. Rainfall pattern in the study area.

Table 1. Variations in precipitation across distinct time intervals.

Return Period/a	Rainfall Depth/mm	Return Period/a	Rainfall Depth/mm
1	51.7	10	99.8
3	74.7	20	114.3
5	85.3	50	133.4

2.4. Calibration and Validation

In order to guarantee a precise depiction of the runoff generation and confluence circumstances within the designated research region, it is imperative to calibrate the model parameters prior to conducting simulation analysis. The selection of Nash–Sutcliffe efficiency (*NSE*) and R^2 as evaluation metrics serves as indicators by which to assess the precision of the model's simulations [26]. This study aims to assess the level of concordance between simulated and measured values, as well as the extent of linear correlation between simulated and measured curves (points).

The *NSE* metric serves as an evaluative tool for assessing the precision of model simulation, with its calculation process being demonstrated in Equation (2):

$$NSE = 1 - \frac{\sum_{i=1}^{n} (Q_{sim,t} - Q_{obs,t})^2}{\sum_{i=1}^{n} (Q_{obs,t} - Q_{avo})^2} \quad (2)$$

where *NSE* is the Nash efficiency coefficient, with a value range less than 1. The larger the value, the better the simulation effect. When *NSE* is less than 0, this indicates poor simulation accuracy; $Q_{sim,t}$ is the simulation value of flow rate at time t; $Q_{obs,t}$ is the monitor value of flow rate at time t; Q_{avo} is the average monitor value of flow rate; and n is the length of the data sequence.

The R^2 statistic serves as a measure that characterizes the magnitude of the association between two variables, and its computation is demonstrated in Equation (3).

$$R^2 = \frac{\left[\sum_{i=1}^{n} (Q_{sim,t} - Q_{avs})(Q_{obs,t} - Q_{avo})\right]^2}{\sum_{i=1}^{n} (Q_{sim,t} - Q_{avs})^2 \times \sum_{i=1}^{n} (Q_{obs,t} - Q_{avo})^2} \quad (3)$$

where R^2 is the correlation coefficient, with a value between 0 and 1 and where the larger this value, the better the simulation effect. Q_{avs} is the average simulation value of flow rate.

The actual monitoring data utilized in this study were derived from the rainfall station at Shandong University within the study area. The precise monitoring locations can be observed in Figure 1. The calibrated results are presented in Figure 5a,b, indicating that all *NSE* values and R^2 values exceeded 0.9. The verified results, displayed in Figure 5c,d, demonstrate *NSE* values surpassing 0.85 and R^2 values exceeding 0.9. Thus, these findings can be effectively employed in subsequent simulation analyses. The specific parameters employed in the model can be found in Table 2.

Table 2. Model parameters of InfoWorks ICM.

Type	Parameter	Rating Results
Production and convergence model	SWMM	SWMM
Runoff coefficient	Roof runoff coefficient	0.75
	Road runoff coefficient	0.80
Confluence parameters (Manning coefficient)	Roof convergence parameters	0.015
	Road confluence parameters	0.015
	Road confluence parameters green space	0.03
Initial losses/m	Initial loss of roof	0.01
	Initial road losses	0.01
	Initial loss of green space	0.015
Horton permeability coefficient	Initial infiltration rate/mm·h^{-1}	100
	steady infiltration rate/mm·h^{-1}	15
	Attenuation rate/1·h^{-1}	2

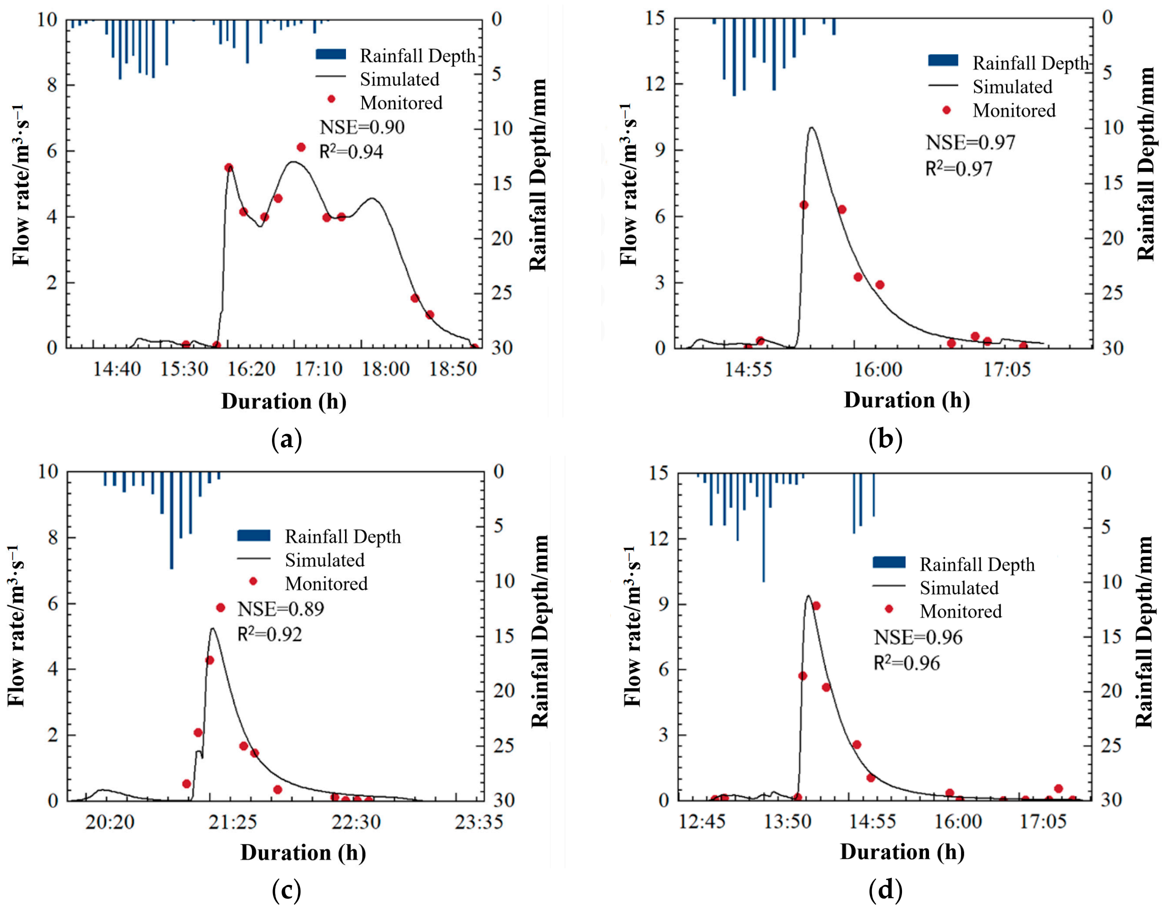

Figure 5. Calibration and validation results of InfoWorks ICM: (**a**) calibration result (6 August 2016), (**b**) calibration result (26 July 2017), (**c**) verification result (6 August 2017), and (**d**) verification result (18 August 2017).

3. Results and Discussion

3.1. Analysis of Stormwater Runoff Reduction Effect in RWSTs under Different Enabling Rules Scenarios

The main evaluation indicators (TVRO, PFR, and PFV) of the stormwater runoff reduction effect under different enabling rules were analyzed. We explored the runoff control effect and its relationship with the threshold values of each rule under three different enabling rule scenarios of RWSTs. Among these, the UCRCV of the RWSTs was set to 300 $m^3 \cdot ha^{-1}$ under enabling rules II and III to determine the optimal rainfall intensity and cumulative rainfall threshold.

3.1.1. Analysis of the TVRO Control Effect

The TVRO of an RWST, under the application of enabling rule I, is depicted in Figure 6a,b. The graph illustrates a decline in TVRO as the UCRCV of the RWST increases. The study area exhibits minimal variation in the influence of different peak proportion coefficients on the TVRO, while the TVRO decreases with an increase in UCRCV. An increase in the UCRCV of the RWSTs from 0 to 500 $m^3 \cdot ha^{-1}$ leads to a significantly higher reduction rate of TVRO during a rainfall event with P = 1a, compared with rainfall events with other return periods. This phenomenon is believed to be caused by the limited capacity of the RWST and its associated water collection infrastructure, which hinders the storage of runoff beyond its maximum capacity and results in the outflow of rainwater. This finding is consistent with the findings of previous studies conducted by Schubert and Snir et al. [27,28]

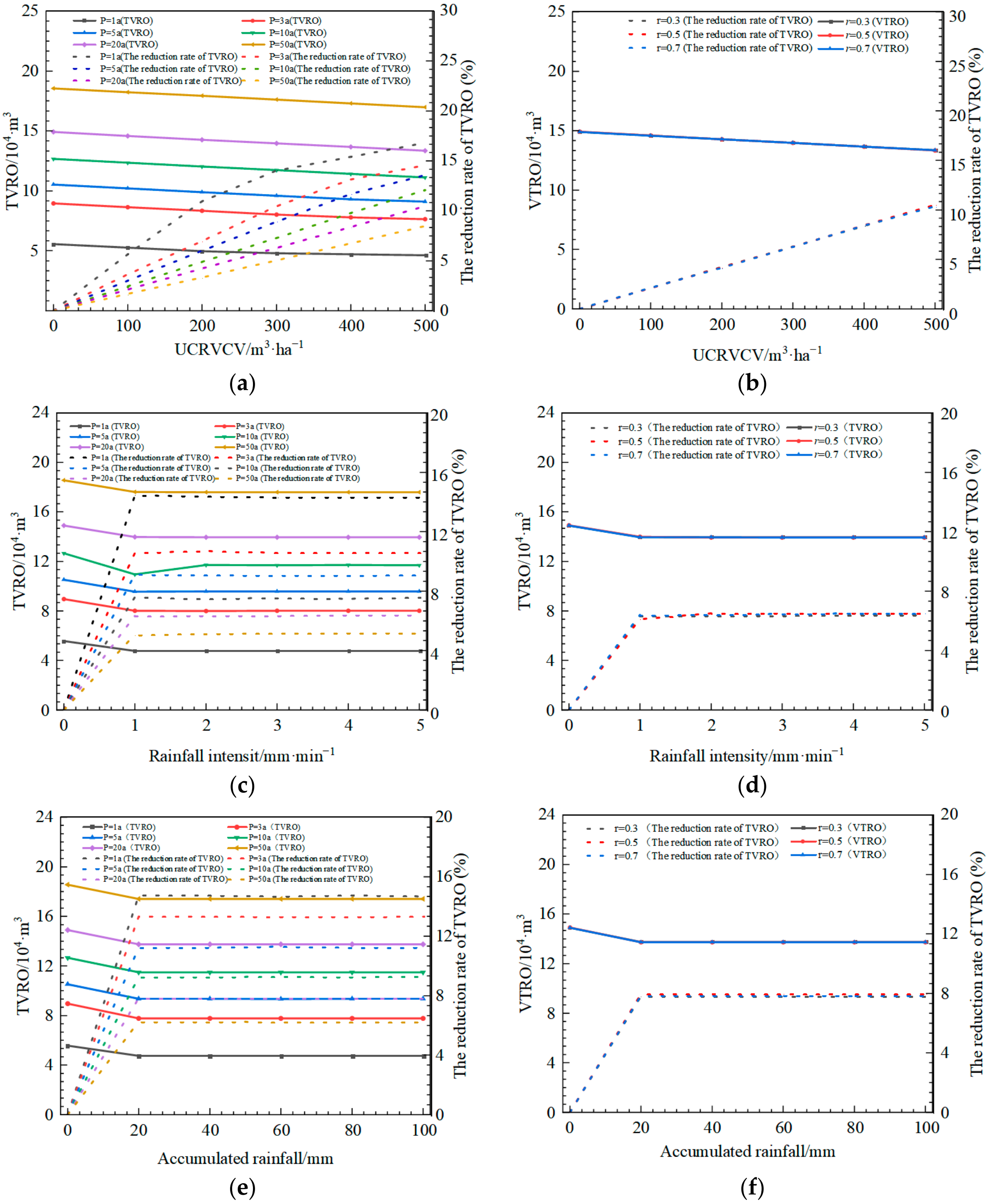

Figure 6. Control effect of TVRO from RWSTs under different enabling rule scenarios. (**a**,**c**,**e**) TVRO at different return periods with enabling rules I, II and III, respectively (P = 1, 3, 5, 10, 20, 50a, r = 0.3). (**b**,**d**,**f**) TVRO at different rain peak coefficients with enabling rules I, II and III, respectively (P = 20a, r = 0.3, 0.5, 0.7).

Figure 6c,d visually depict the performance of the TVRO under the influence of enabling rule II. Upon analyzing Figure 6c, it becomes evident that the TVRO does not display a significant trend as the threshold for rainfall intensity rises. However, significant distinctions were noted, particularly in the form of a substantial decrease in the TVRO during the rainfall intensity threshold of 0–1 mm·min^{-1}. The TVRO exhibited a recovery within the range of 1–2 mm·min^{-1} and subsequently stabilized without further modifications within the range of 2–5 mm·min^{-1}. In this study, it was observed that the implementation of enabling rule II demonstrated a more effective regulation of the TVRO across various return periods of rainfall events when the threshold of rainfall intensity was set at 1 mm·min^{-1}. The study observed that the reduction rates of TVRO during rainfall events with P = 1, 3, 5, 10, 20, 50a were determined to be 14.45%, 10.59%, 9.13%, 7.60%, 6.33%, and 5.06%, respectively. It is plausible to consider that the excessively elevated threshold for rainfall intensity might account for this phenomenon. When rainfall intensity surpasses 2 mm·min^{-1}, the RWSTs system remains inactive. Consequently, there is a failure to optimize storage capacity utilization and mitigate runoff outflow. Figure 6d demonstrates a decreasing trend in TVRO as the threshold for rainfall intensity increases across different scenarios of rainfall events that are characterized by varying peak proportion coefficients. However, the impact of these coefficients on TVRO is considered to be insignificant. The study documents the average rates of reduction in total external emissions at peak proportion coefficients of r = 0.3, 0.5, and 0.7 as 6.37%, 6.44%, and 6.46%, respectively. The main reason for such situations is that the occurrence of TVRO is influenced by rainfall intensity and has little correlation with the peak proportion coefficient [29]. Therefore, enabling rule II has the same optimal rainfall intensity threshold range for different design rainfall events.

Figure 6e,f present portrayals of TVRO that depend on the implementation of enabling rule III. The graph visually shows a significant decrease in TVRO as the cumulative rainfall threshold for the RWST increases. The optimal operating time for an RWST is when the rainfall approaches or reaches its peak. The larger the return period of a rainfall event, the greater the cumulative rainfall before the rainfall approaches or reaches its peak, and the smaller the threshold for optimal cumulative rainfall activation. The effectiveness of an RWST is maximized when rainfall is approaching or at its peak level, particularly as the return period of a rainfall event increases. The larger the recurrence period of a rainfall event, the higher the total rainfall before it reaches its peak, and the lower the threshold for achieving the optimal cumulative rainfall [29].

3.1.2. Analysis of the PFR Control Effect

The PFR pattern of RWSTs under various enabling rules is illustrated in Figure 7. Analysis of Figure 7a,b reveals that the PFR of rainwater outflow decreases as the UCRCV of the RWSTs increases. This can be attributed to the fact that the regulatory impact of PFR has reached or approached its optimal level at a unit catchment area regulation volume of 300 m^3·ha^{-1}, which allows for maximum collection and storage of rainwater runoff. However, as the UCRCV continues to increase, the PFR has reached its lowest level and is unable to decrease further. The control effect of PFR is not significant when the UCRCV of the RWSTs is less than 0 m^3·ha^{-1}, 100 m^3·ha^{-1}, and 200 m^3·ha^{-1} for respective peak proportion coefficients of 0.3, 0.5, and 0.7. In situations where the peak proportion coefficient is relatively high, the capacity of the RWSTs becomes saturated before reaching the peak, resulting in an insignificant reduction of PFR.

Based on the observations from Figure 7c,d, it is evident that the progressive rise in the rainfall intensity threshold of the activated RWSTs leads to a general decline followed by a slight increase in the PFR. This analysis is supported by the fact that when the rainfall intensity threshold reaches the range of 4–5 mm·min^{-1}, the RWST enables efficient utilization of storage capacity, resulting in a reduction in the PFR and successful attainment of PFR reduction effects. These findings align with the research conducted by Xu et al. [30]. As the intensity of rainfall surpasses a certain threshold, the PFR exhibits a consistent trend across various scenarios of rainfall events characterized by different peak proportion coefficients. Notably, when the peak proportion coefficients are set at r = 0.3 and 0.5, the optimal control effect of PFR is observed at a rainfall intensity threshold of 1 mm·min^{-1}. However, as the value of r increases to 0.7, the reduction rate of PFR demonstrates an upward trend in correlation with the escalation of the rainfall intensity threshold. When the rainfall intensity threshold falls within the range of 1 mm·min^{-1}, the activation of enabling rule II yields the most effective control over PFR during diverse rainfall events characterized by varying peak proportion coefficients [23].

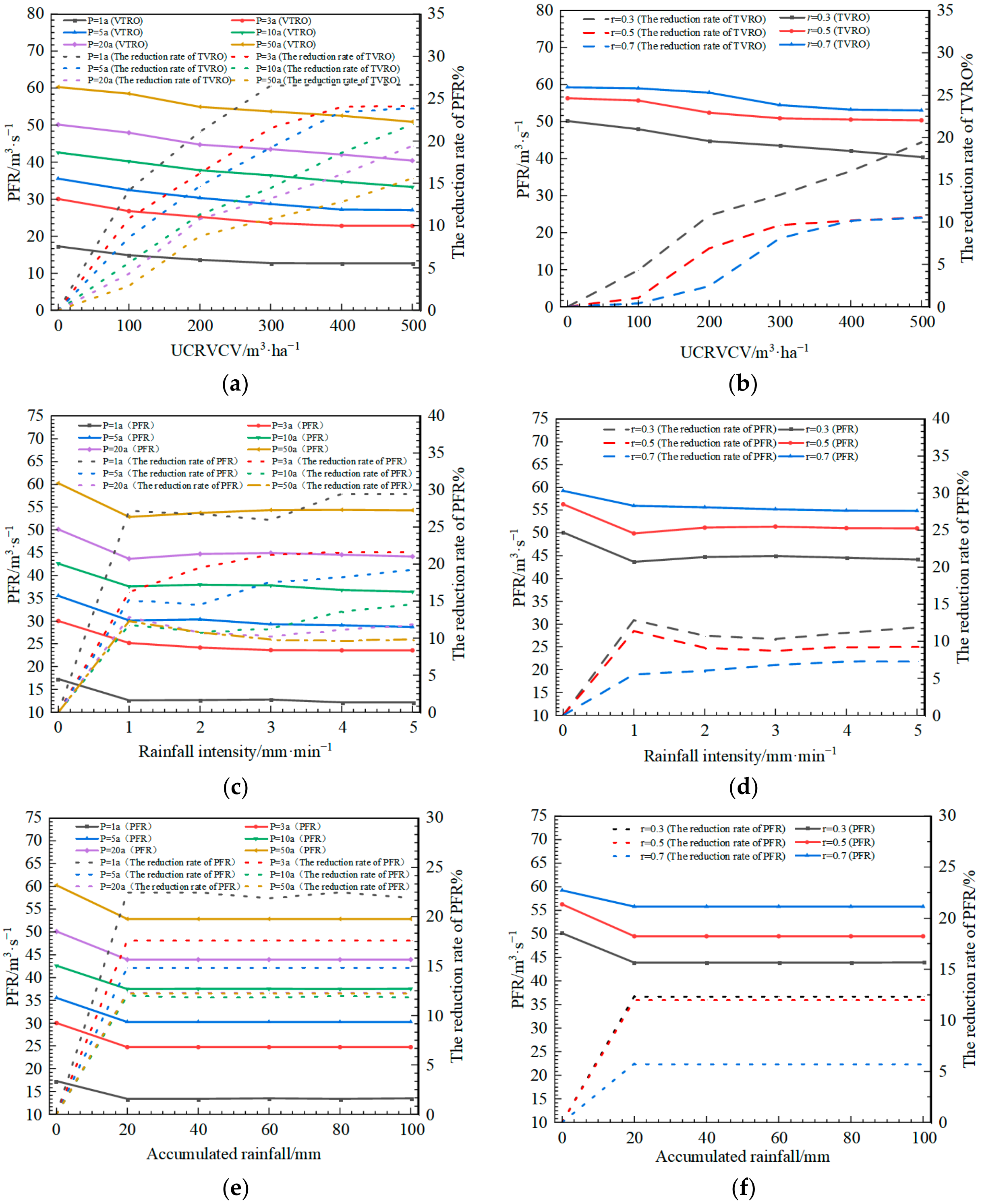

Figure 7. PFR control effect of RWSTs under different enabling rule scenarios. (**a**,**c**,**e**) PFR at different return periods with enabling rules I, II and III, respectively (P = 1, 3, 5, 10, 20, 50a, r = 0.3). (**b**,**d**,**f**) PFR at different rain peak coefficients with enabling rules I, II and III, respectively (P = 20a, r = 0.3, 0.5, 0.7).

Based on the observations from Figure 7e,f, it is evident that there is a decreasing trend in the PFR as the cumulative rainfall threshold for enabling rule III increases. Additionally, this trend is consistent across different return periods of rainfall. As the cumulative rainfall threshold increases, the PFR exhibits a consistent decreasing trend across various scenarios of peak proportion coefficient rainfall events. A smaller peak proportion coefficient corresponds with a more pronounced reduction effect. Specifically, the PFR reduction rate surpasses 12% for rainfall events with r = 0.3 and 0.5, whereas it is merely 5.77% for rainfall events with r = 0.7. The optimal threshold for activating cumulative rainfall for PFR control is 20 mm under rainfall events with peak proportion coefficients of 0.3, 0.5, and 0.7.

3.1.3. Analysis of the PFV Control Effect

Based on the observations from Figure 8a,b, it is evident that the PFV of enabling rule I exhibits a decline as the UCRCV of the RWSTs increases. Furthermore, the PFV gradually decreases as the return period increases, while keeping the conditions constant. The reduction effect of the P = 1, 3, and 5a rainfall event is considerably superior to that of the P = 10, 20, and 50a rainfall event, primarily due to the ample regulating capacity of the RWST system. This capacity enables the efficient mitigation of substantial rainwater runoff and discharge and aligns with the research findings of Liang and Matteo et al. [23,24]. As the UCRCV of the RWSTs increases, the PFV control effect becomes increasingly pronounced, as indicated by peak proportion coefficients of 0.3, 0.5, and 0.7. Notably, rainfall events characterized by smaller peak proportion coefficients exhibit significantly superior control effects compared with those with larger peak proportion coefficients. This phenomenon can be attributed to the positive correlation between the peak proportion coefficient and the accumulation of rainfall prior to reaching its peak. Consequently, enabling rule I exhibits distinct optimal thresholds, dependent on the nature of the rainfall event. In general, a higher threshold is required for the optimal activation of the UCRCV when the rainfall return period is longer or when the peak rainfall is delayed.

From Figure 8c,d, it can be seen that, with the increase of the rainfall intensity threshold for enabling rule II to activate the RWST, the PFV generally shows a decreasing trend, and rainfall at different return periods shows a similar trend. The overall PFV reduction rate shows a trend of first decreasing and then increasing. As the threshold of rainfall intensity increases, there is a slight difference in the reduction rate of PFV for different return periods of rainfall events. The smaller the return period, the better the reduction effect of PFV. The reason for this is that, when the threshold of rainfall intensity increases to the range of 4 mm$\cdot$min^{-1}, the RWST can be activated, which in turn allows for the effective utilization of the storage space of the RWST to regulate excess runoff, thereby reducing the PFV and reducing the risk of water safety incidents caused by excessive PFV. As the threshold of rainfall intensity increases, the PFV under different peak proportion coefficient rainfall event scenarios shows the same trend. When the peak proportion coefficient r = 0.3 and 0.5, the PFV control effect is best at the rainfall intensity threshold of 1 mm$\cdot$min^{-1}. However, when r = 0.7, the PFV reduction rate increases with the increase of rainfall intensity threshold. As the threshold for rainfall intensity increases, the rate of PFV reduction shows an upward trend. When the rainfall intensity threshold is within the range of 1 mm$\cdot$min^{-1}, enabling rule II shows the best control effect on PFV under different peak proportion coefficient rainfall events.

Based on the observations from Figure 8e,f, it is evident that there is a general decline in the PFV as the cumulative rainfall threshold for enabling rule III increases. Additionally, the rainfall at various return periods exhibits a comparable pattern. There exists a cumulative rainfall activation threshold of 20 mm that maximizes the flow rate control effect under rainfall events of P = 1, 3, 5, 10, 20, and 50a. As the threshold for cumulative rainfall increases, there is a consistent decreasing trend in the PFV under various peak proportion coefficient rainfall event scenarios. It is observed that a smaller peak proportion coefficient results in a more favorable reduction effect. Specifically, for rainfall events with peak proportion coefficients of 0.3, 0.5, and 0.7, the optimal threshold for activating cumulative rainfall is determined to be 20 mm.

In summary, enabling rules I, and II have different thresholds for TVRO, PFR, and PFV under rainfall events at different return periods. When their threshold of UCRCV and rainfall intensity are greater than 300 $m^3 \cdot ha^{-1}$ and 1 $mm \cdot min^{-1}$, respectively, the growth trends of TVRO, PFR, and PFV decrease. The TVRO, PFR, and PFV of enabling rule III showed no significant fluctuations after the accumulated rainfall exceeded 20 mm. Therefore, the optimal thresholds for UCRCV, rainfall intensity, and accumulated rainfall for enabling rules I, II, and III are determined to be 300 $m^3 \cdot ha^{-1}$, 1 $mm \cdot min^{-1}$, and 20 mm, respectively.

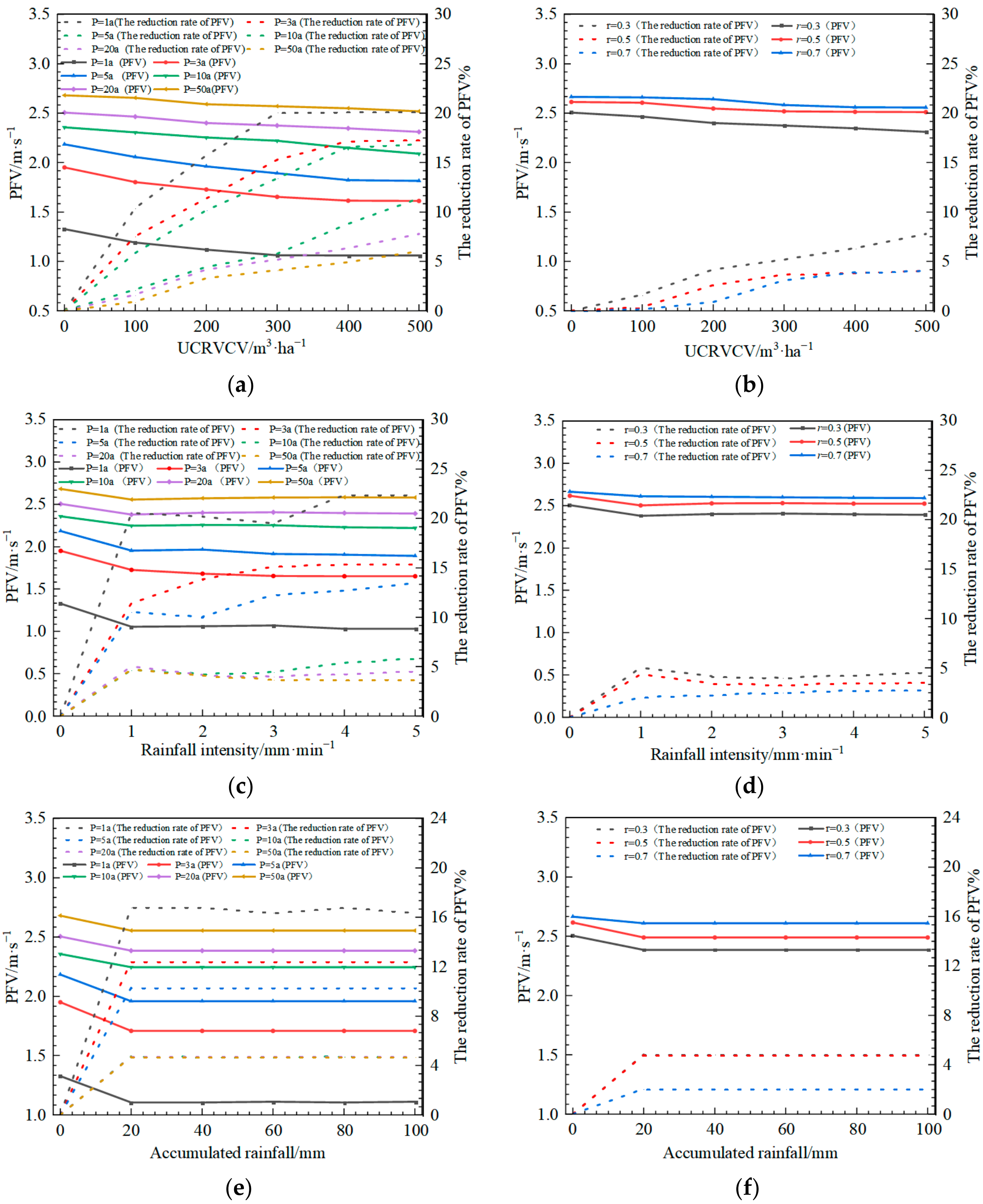

Figure 8. Effect of RWST flow control in different enabling rule scenarios. (**a**,**c**,**e**) PFV at different return periods with enabling rules I, II and III, respectively (P = 1, 3, 5, 10, 20, 50a, r = 0.3). (**b**,**d**,**f**) PFV at different rain peak coefficient with enabling rules I, II and III, respectively (P = 20a, r = 0.3, 0.5, 0.7).

3.2. Optimization of Enabling Rule for Different RWSTs

To facilitate a comprehensive analysis and elucidation of the optimal control outcomes associated with enabling rules I, II, and III, three distinct types of enabling rules were implemented for RWSTs with a UCRCV value of 300 $m^3 \cdot ha^{-1}$. The rainfall intensity threshold of 1 $mm \cdot min^{-1}$ and the cumulative rainfall threshold of 20 mm were identified as the optimal enabling thresholds for enabling rules II and III, respectively. To determine the most suitable enabling rule for optimizing and controlling the TVRO, PFR, and PFV, two actual rainfall events in Jinan city were simulated and verified.

A comparison of the control effect of TVRO under different RWSTs enabling rules is illustrated in Figure 9. Based on the findings from Figure 9, it is evident that the overall comparison of the three enabling rules indicates that enabling rule III yields a superior TVRO control effect compared with the other enabling rules. The control effect of various RWSTs enabling rules on TVRO decreases as the return period increases. The findings indicate that, across different design rainfall events (P = 1, 3, 5, 10, 20, 50a, r = 0.3), enabling rule III demonstrates superior control effectiveness compared with enabling rule I and enabling rule II. Additionally, enabling rule II exhibits slightly lower control effectiveness than enabling rule I. The TVRO's reduction rates, as determined by the application of enabling rule III across various return periods (P = 1, 3, 5, 10, 20, 50a, r = 0.3), are 14.75%, 13.32%, 11.23%, 9.25%, 7.81%, and 6.25%, respectively.

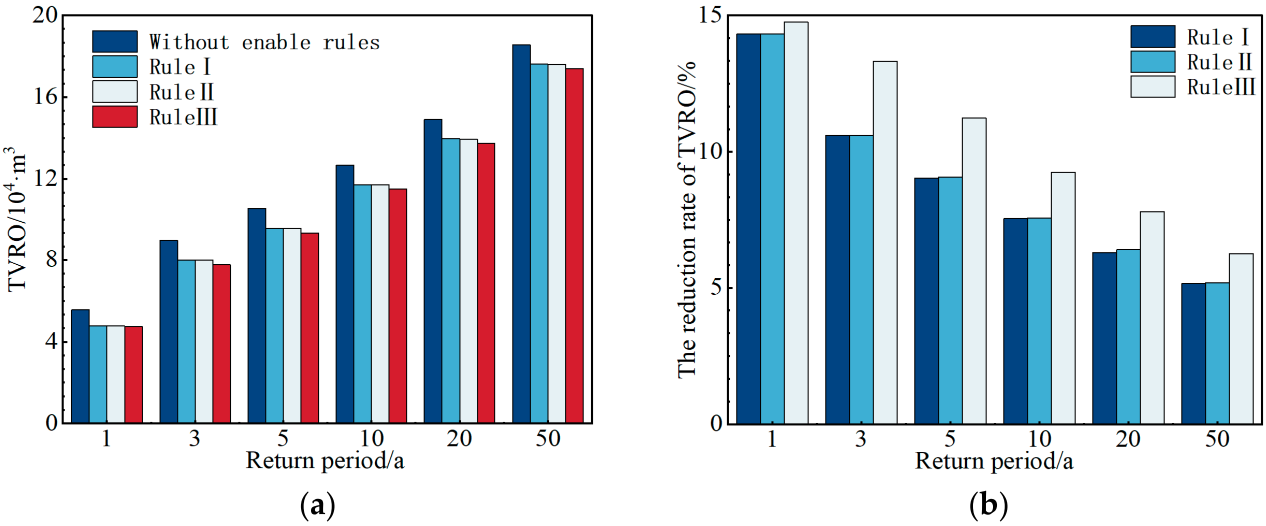

Figure 9. Comparison of TVRO under different enabling rules of RWSTs (P = 1, 3, 5, 10, 20, 50a, r = 0.3). (**a**) Effect of TVRO control and (**b**) reduction rate of total external emissions.

Figure 10 illustrates the comparison of the effects of PFR control under various RWST enabling rules. Based on the findings from Figure 10, it is evident that enabling rule II outperforms the other enabling rules in terms of PFR control effectiveness. Furthermore, the PFR control effect exhibits a consistent trend across different RWST enabling rules, wherein it diminishes as the return period increases. The findings indicate that the implementation of enabling rule II yielded superior control effects compared with enabling rule I and enabling rule III during the design rainfall events of P = 1, 3, 5, and 10a. However, enabling rule II exhibited a slight disadvantage in comparison with enabling rule I and enabling rule III under the design rainfall events P = 20 and 50a, enabling rule III produced better PFR control effects. The PFR reduction rates achieved by utilizing enabling rule II varied across return periods (P = 1, 3, 5, 10, 20, 50a, r = 0.3), with rates of 29.49%, 21.65%, 19.25%, 14.57%, 11.84%, and 9.84% respectively.

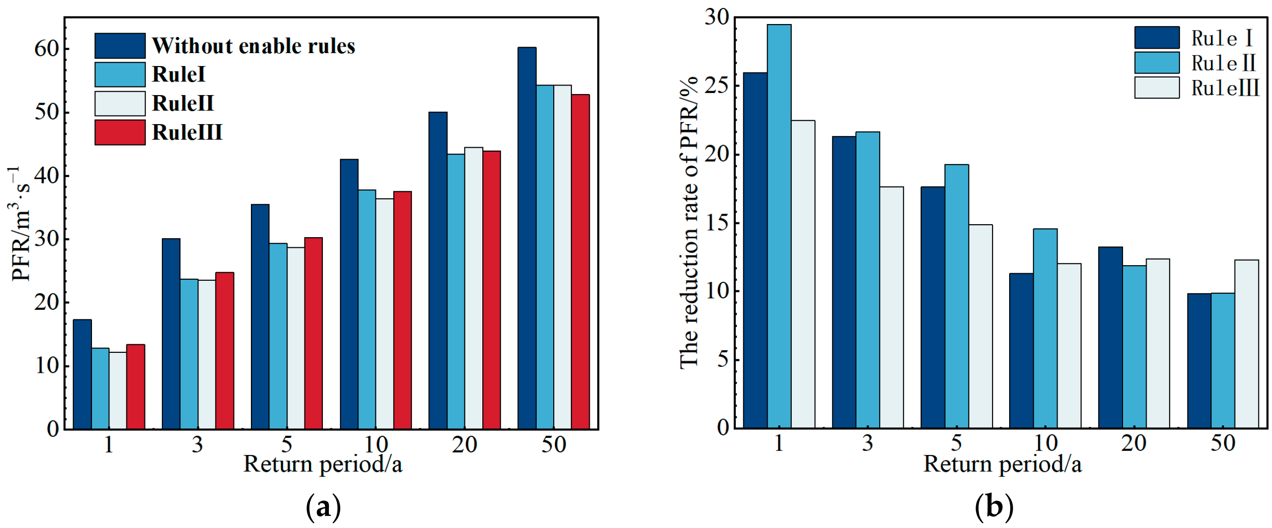

Figure 10. Comparison of PFR under different enabling rules of RWSTs (P = 1, 3, 5, 10, 20, 50a, r = 0.3). (**a**) PFR control effect and (**b**)PFR reduction rate.

Figure 11 illustrates a comparison of the control effects of PFV under various RWST enabling rules. It is evident from Figure 11 that enabling rule II shows a consistent trend in PFV and PFR control effects, that is, in rainfall events with P = 1, 3, 5 and 10a, the PFV control effect with enabling rule II is the best. Under the design rainfall events of P = 20 and 50a, the PFV control effect is as follows: enabling rule III > enabling rule II > enabling rule I. The reduction rates of PFV achieved by enabling rule II were seen to vary across different return periods (P = 1, 3, 5, 10, 20, 50a, r = 0.3), with observed reduction rates of 22.36%, 15.38%, 13.46%, 5.85%, 4.59%, and 3.73%, respectively.

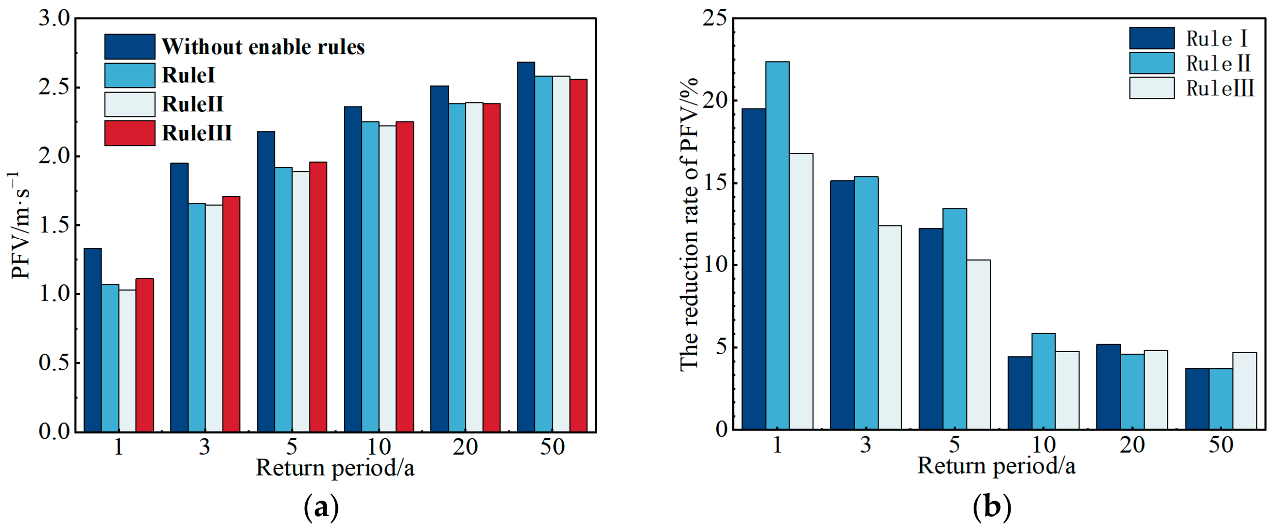

Figure 11. Comparison of PFV under different enabling rules of RWSTs (P = 1, 3, 5, 10, 20, 50a, r = 0.3). (**a**) PFV control effect and (**b**) PFV reduction rate.

In summary, enabling rule III has more advantages in rainwater runoff regulation and is more effective than enabling rule II. That is, enabling rule II only showed the best PFR and PFV control effects in P = 1, 3, 5, and 10a rainfall events, while enabling Rule III showed the best TVRO, PFR, and PFV control effects in all other rainfall events.

The historical rainfall data were utilized to provide additional confirmation of the runoff control efficacy of the optimal enabling rule and its corresponding threshold, as demonstrated by two monitored rainfall events within the study area. The verification outcomes of these two actual rainfall events are depicted in Figure 12. It was observed that, under the three enabling rules, the TVRO, PFR, and PFV were effectively regulated during both rainfall events.

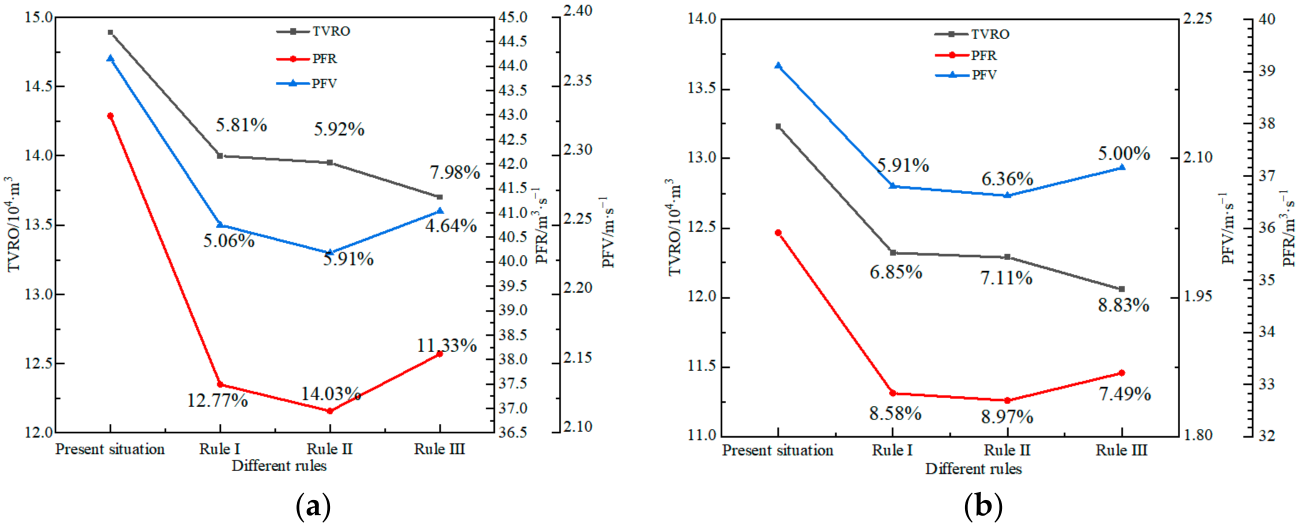

Figure 12. Performance of enabling rules of different RWSTs: (**a**,**b**) represent the control effects of TVRO, PFR, and PFV on 1 August 2016 and 14 August 2016, respectively.

In the rainfall event that occurred on 1 August 2016 (Figure 12a), the implementation of enabling rule III was demonstrated the most effective control on the TVRO. The utilization of enabling rules I, II, and III resulted in reductions of 5.81%, 5.92%, and 7.98% respectively, in comparison with the prevailing conditions. In terms of PFR, enabling rule II exhibited the most significant control effect, leading to reductions of 12.77%, 14.03%, and 11.33% for enabling rules I, II, and III, respectively, when compared with the current situation. Similarly, for PFV, the implementation of enabling rule II yielded the most effective control effect, resulting in reductions of 5.06%, 5.91%, and 4.64% for enabling rules I, II, and III, respectively, in comparison with the current situation.

The rainfall event that occurred on 14 August 2016 (Figure 12b) showed a consistent trend with the rainfall event on 1 August 2016 (Figure 12a). Overall, the control effect of the two actual rainfall events is consistent with the above conclusion. That is, enabling rule III has an advantage in controlling the TVRO, with enabling rule III being more effective than enabling rule II, and enabling rule II being more effective than enabling rule I. The control effect of enabling rule II on PFR and PFV is either better or similar to the other two enabling rules.

In summary, it can be determined that enabling rule III has the greatest advantage in improving stormwater runoff reduction within the study area, thereby reducing TVRO. Its optimal threshold for activating an RWST is when the accumulated rainfall reaches 20 mm. The above activation threshold evaluation and determination methods can be used to construct a stormwater runoff reduction pattern from the large watershed scale, including the determination of RWST location, size, and control threshold, and other operating modes. This provides an important theoretical basis for the study of future waterlogging control and urban disaster prevention in the study area.

4. Conclusions

At present, in the global rainwater control work, a large number of RWSTs are constructed for rainwater regulation, and a large number of solutions have been proposed, but the results are very limited. The best control strategy for large-watershed-scale rainwater runoff is still lacking; this is especially so for a method and technical system by which to adjust the RWST RTC scheme and improve the reduction effect of excessive rainwater runoff. This still requires sufficient research. Therefore, exploring the optimal solution for the RTC of large-watershed-scale RWSTs is of great significance.

This study proposes a method for optimizing the activation threshold of RWSTs, applying the RTC function of the InfoWorks ICM model in order to evaluate the TVRO, PFR, and PFV control effects of RWSTs under three enabling rules (a total of 162 simulation scenarios). The optimal enabling rule and corresponding activation threshold were determined, and the runoff control effect of an RWST was further evaluated using actual rainfall data. It has been confirmed that the optimal enabling rule with the greatest impact when improving the efficiency of rainwater runoff reduction in the study area is enabling rule III, and that the corresponding optimal threshold by which to activate RWST is met when the accumulated rainfall reaches 20 mm. Meanwhile, the control effects of three enabling rules on TVRO, PFR, and PFV were also explored. Enabling rule II displays the maximum control over PFR and PFV, while enabling rule III displays the most effective control over TVRO. The construction of this method can improve the flood control capacity of the research area and the large-watershed-scale rainwater runoff control mode, providing an important theoretical basis and a technical system for future waterlogging control work in the research area.

In future waterlogging control work, the abovementioned rainwater runoff control work can be carried out in different areas. It could be utilized to analyze the runoff regulation effects among various RWSTs and adopt different enabling rules and thresholds for each region in order to achieve free control of TVRO, PFR, PFV, and cross regional runoff transfer. It is conducive to the establishment of a large-watershed-scale rainwater runoff control technology system and optimal RTC schemes, and may help to create further scientific plans for rainwater control around the world. This may provide a reasonable reference method for evaluating the efficiency of RWSTs worldwide and determining an optimal RTC scheme.

Author Contributions: Conceptualization, G.M. and K.T.; methodology, Y.G. and G.M.; software, G.M. and K.T.; validation, K.T. and Z.L.; formal analysis, Z.L.; resources, Y.G.; writing—original draft preparation, G.M. and K.T.; writing—review and editing, Y.G., G.M. and K.T. All authors have read and agreed to the published version of the manuscript.

Funding: This research was funded by the National Key R&D Program of China (grant no. 2022YFC3800500) and the Project of Construction and Support for High-Level Innovative Teams of Beijing Municipal Institutions (BPHR20220108).

Data Availability Statement: The data presented in this study is available on request from the corresponding author.

Conflicts of Interest: The authors declare no conflict of interest.

References

1. Booth, D.B.; Roy, A.H.; Smith, B.; Capps, K.A. Global perspectives on the urban stream syndrome. *Freshw. Sci.* **2016**, *35*, 412–420. [CrossRef]
2. Wang, Q.; Ma, Z.; Yuan, X.; Wang, J.; Mu, Z.; Zuo, J.; Zhang, J.; Hong, J.; Wang, S. Is cement pavement more sustainable than permeable brick pavement? A case study for Jinan, China. *J. Clean. Prod.* **2019**, *226*, 306–315. [CrossRef]
3. Hadidi, A.; Holzbecher, E.; Molenaar, R.E. Flood mapping in face of rapid urbanization: A case study of Wadi Majraf-Manumah, Muscat, Sultanate of Oman. *Urban Water J.* **2020**, *17*, 407–415. [CrossRef]
4. Kam, P.M.; Aznar, G.; Schewe, J.; Milano, L.; Ginnetti, J.; Willner, S.; McCaughey, J.W.; Bresch, D.N. Global warming and population change both heighten future risk of human displacement due to river floods. *Environ. Res. Lett.* **2021**, *16*, 044026. [CrossRef]
5. Breinl, K.; Lun, D.; Müller-Thomy, H.; Blöschl, G. Understanding the relationship between rainfall and flood probabilities through combined intensity-duration-frequency analysis. *J. Hydrol.* **2021**, *602*, 126759. [CrossRef]
6. Trigg, M.A.; Birch, C.E.; Neal, J.C.; Bates, P.D.; Smith, A.; Sampson, C.C.; Yamazaki, D.; Hirabayashi, Y.; Pappenberger, F.; Dutra, E.; et al. The credibility challenge for global fluvial flood risk analysis. *Environ. Res. Lett.* **2016**, *11*, 094014. [CrossRef]
7. Centre for Research on the Epidemiology of Disasters; UN Office for Disaster Risk Reduction. *The Human Cost of Disasters: An Overview of the Last 20 Years (2000–2019)*; Centre for Research on the Epidemiology of Disasters: Brussels, Belgium; UN Office for Disaster Risk Reduction: Geneva, Switzerland, 2020.
8. Willner, S.N.; Levermann, A.; Zhao, F.; Frieler, K. Adaptation required to preserve future high-end river flood risk at present levels. *Sci. Adv.* **2018**, *4*, eaao1914. [CrossRef] [PubMed]

9. Hu, J.; Zhao, B.; Liu, X.; Cao, D.; Guo, X.; Xu, X.; Xu, T. Assessment of Drainage Capacity and Waterlogging Risk in Central Zone of Zhenjiang City. *China Water Wastewater* **2015**, *31*, 100–108.
10. Ministry of Water Resources of the People's Republic of China. *China Flood and Drought Disaster Prevention Bulletin 2022*; China Water & Power Press: Beijing, China, 2022; Volume 25.
11. Cheng, T.; Huang, B.; Yang, Z.; Qiu, J.; Zhao, B.; Xu, Z. On the effects of flood reduction for green and grey sponge city measures and their synergistic relationship—Case study in Jinan sponge city pilot area. *Urban Clim.* **2022**, *42*, 101058. [CrossRef]
12. Chen, T.; Lin, Z. Planning for climate change: Evaluating the changing patterns of flood vulnerability in a case study in New Taipei City, Taiwan. *Stoch. Environ. Res. Risk Assess* **2021**, *35*, 1161–1174. [CrossRef]
13. Ali, R.; Kuriqi, A.; Kisi, O. Human–Environment Natural Disasters Interconnection in China: A Review. *Climate* **2020**, *8*, 48. [CrossRef]
14. Xia, J.; Zhang, Y.; Xiong, L.; He, S.; Wang, L.; Yu, Z. Opportunities and challenges of the Sponge City construction related to urban water issues in China. *Sci. China Earth Sci.* **2017**, *60*, 652–658. [CrossRef]
15. Li, Q.; Wang, F.; Yu, Y.; Huang, Z.; Li, M.; Guan, Y. Comprehensive performance evaluation of LID practices for the sponge city construction: A case study in Guangxi, China. *J. Environ. Manag.* **2019**, *231*, 10–20. [CrossRef]
16. Leng, L.; Mao, X.; Jia, H.; Xu, T.; Chen, A.S.; Yin, D.; Fu, G. Performance assessment of coupled green-grey-blue systems for Sponge City construction. *Sci. Total Environ.* **2020**, *728*, 138608. [CrossRef]
17. Rizzo, A. Hybrid Approach for Excess Stormwater Management: Combining Decentralized and Centralized Strategies for the Enhancement of Urban Flooding Resilience. *Water* **2021**, *13*, 3635.
18. Zhang, J.; Gao, X.; Zhang, P.; Wang, Y.; Huang, S.; Lin, G. Field tests on Fiber-Reinforced Plastic (FRP) stormwater storage tank under road pavement for "Spong City" development. *Case Stud. Constr. Mater.* **2023**, *18*, e02097. [CrossRef]
19. Dąbrowski, W.; Nowak, M. Potential of storm water storage tank outflow construction in the prevention of sewerage overload. *Appl. Water Sci.* **2022**, *12*, 205. [CrossRef]
20. Wang, M.; Sun, Y.; Sweetapple, C. Optimization of storage tank locations in an urban stormwater drainage system using a two-stage approach. *J. Environ. Manag.* **2017**, *204*, 31–38. [CrossRef] [PubMed]
21. Wang, M.; Li, M.; Sweetapple, C. A new framework for distributed storage tanks placement based on a resilience characteristic metric and reduced modelling. *J. Environ. Manag.* **2023**, *342*, 118098. [CrossRef] [PubMed]
22. Wang, S.; Wang, J.; Xue, C.; Qiu, R.; Sun, S.; Yang, Z.; Qiao, Y. Assessing the effectiveness of a residential-scale detention tank operated in a multi-objective approach using SWMM. *Water Sci. Technol.* **2023**, *89*, 54–70. [CrossRef] [PubMed]
23. Liang, R.; Di Matteo, M.; Maier, H.R.; Thyer, M.A. Real-Time, Smart Rainwater Storage Systems: Potential Solution to Mitigate Urban Flooding. *Water* **2019**, *11*, 2428. [CrossRef]
24. Matteo, M.D.; Liang, R.; Maier, H.R.; Thyer, M.A.; Simpson, A.R.; Dandy, G.C.; Ernst, B. Controlling rainwater storage as a system: An opportunity to reduce urban flood peaks for rare, long duration storms. *Environ. Model. Softw.* **2019**, *111*, 34–41. [CrossRef]
25. Jinan Municipal Engineering Design & Research Institute (Group) Co., Ltd.; Jinan Layout Design Research Institute. The Comprehensive Planning of Urban Drainage (Rainwater) and Waterlogging Prevention in Jinan. 2019; *Unpublished work*.
26. Al-Safi, H.I.J.; Sarukkalige, P.R. The application of conceptual modelling to assess the impacts of future climate change on the hydrological response of the Harvey River catchment. *J. Hydro-Environ. Res.* **2020**, *28*, 22–33. [CrossRef]
27. Schubert, J.E.; Burns, M.J.; Fletcher, T.D.; Sanders, B.F. A framework for the case-specific assessment of Green Infrastructure in mitigating urban flood hazards. *Adv. Water Resour.* **2017**, *108*, 55–68. [CrossRef]
28. Snir, O.; Friedler, E.; Ostfeld, A. Optimizing the Control of Decentralized Rainwater Harvesting Systems for Reducing Urban Drainage Flows. *Water* **2022**, *14*, 571. [CrossRef]
29. Chen, W.; Huang, G.; Zhang, H.; Wang, W. Urban inundation response to rainstorm patterns with a coupled hydrodynamic model: A case study in Haidian Island, China. *J. Hydrol.* **2018**, *564*, 1022–1035. [CrossRef]
30. Xu, W.D.; Fletcher, T.D.; Duncan, H.P.; Bergmann, D.J.; Breman, J.; Burns, M.J. Improving the Multi-Objective Performance of Rainwater Harvesting Systems Using Real-Time Control Technology. *Water* **2018**, *10*, 147. [CrossRef]